Advances in Machinery, Materials Science and Engineering Application
M. Chen et al. (Eds.)

doi:10.3233/ATDE220459

Research on Dynamic Modeling and Cable Tension Optimization of Marine Cable-Driven Parallel Cleaning Robot

Jian LI [a], Yizong CHEN [a], Shenghai WANG [a,1], Guangdong HAN [a], Yuqing SUN [a] and Weirong LUO [a]
[a] *College of Marine Engineering, Dalian Maritime University, Dalian 116026, China*

Abstract. Ship cleaning is mainly done manually, which is high operation risk and low work efficiency. For that, it is proposed to apply the cable-driven parallel robot to the field of ship cleaning. The related research of the traditional cable-driven parallel robot is mainly focused on the fixed base, which largely ignores the influence of the base motion on its work performance. Considering the influence of ship motion caused by wave excitation on modeling accuracy, the dynamic model of the system is established by Newton-Euler method. And then, the least variance method of correlation force was used to optimize the cable tension. Finally, the correctness and rationality of the proposed theory are verified by Simulink-Adams co-simulation. The simulation results show that the trajectory comparison effect is good, which verifies the accuracy and validity of the proposed theory.

Keywords. CDPR, ship cleaning, dynamic model, tension optimization

1. Introduction

Currently, ship cleaning is mainly done by the operator using tools such as hammers, chemicals and high-pressure water guns, which has the disadvantages of low automation, low work efficiency and limited scope of operation [1,2]. The ship will shake under the excitation of waves, and there is a risk of falling when the operator is cleaning at a high position, which greatly challenges the safety of personnel. Therefore, it is inevitable to develop a cleaning automation equipment.

Cable-driven parallel robot (CDPR) is a device that transfers the motion of the motor to the end-effector with the cable as the driving part [3]. Because they have characteristics of high load, large working space, fast movement and easy disassembly, CDPRs are widely used in medical, industrial and military fields [4-6]. Jiang [7] proposed an analytical algorithm to solve the coordinated transport of multiple overhead robot suspension loads. Horoub [8] proposed a cable-driven marine platform with the Stewart-Gough parallel robot as the support structure. In view of the above application, this paper proposes to apply the technology of cable-driven cleaning parallel robot (CDPCR) to field of ship maintenance.

[1] Shenghai Wang, Corresponding author, College of Marine Engineering, Dalian Maritime University, Dalian 116026, China; E-mail: shenghai_wang@dlmu.edu.cn.

In order to improve the overall control accuracy of the CDPR system, the more accurate dynamic model needs to be established. Jamshidifar [9] proposed a dynamic model considering end-effector vibration. Du [10] used Hamilton's principle to propose a dynamic model of a large-span CDPR in space. Zhao [11] proposed dynamic model of underwater camera stabilization platform based on Newton Euler method. The traditional dynamic model mainly solves the problem of fixed base, but rarely consider the influence of ship motion on CDCPR. Therefore, the dynamic model of CDPCR was established based on Newton-Euler method, which considered the influence of ship movement on operation.

For the cable tension optimization algorithm of the CDPR, the relevant researchers have also carried out extensive research. Pott [12] used the closed solution of vector to optimized tension, but the scope of application is limited. Borgstrom [13] used the least 2-norm method to optimize tension, but the stiffness of the optimized system is limited. In this paper, the minimum variance method is used to optimize the cable tension. The optimized cable tension has good continuity and real-time performance.

The chapter structure of the paper is arranged as follows. In the second part, the structure of CDPCR is introduced. The third part derived the dynamic model of CDPCR, and the least variance method is proposed to optimize the cable tension. In the fourth part, the accuracy of the model is verified by Simulink-Adams co-simulation. The fifth part summarizes the research conclusions.

2. Structure of CDPCR

The structural components of CDPCR is shown in figure 1, the four-cable-driven parallel robot is adopted. The prototype model is mainly composed of motion platform, driving motors, frame, tension sensors, encoders, cable disorder prevention devices and bucket. Among them, tension sensor is used to measure cable tension value in real time. The cable disorder prevention device can prevent cable disorder during cleaning operation.

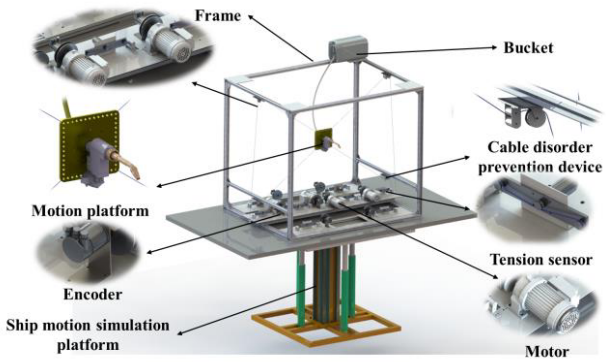

Figure 1. 3D model of the prototype.

3. Dynamic Modeling of CDPCR

3.1. Kinematic Model

In this paper, the pose conversion relationship between frame is set as $\boldsymbol{X}_{ij}^{j}=\begin{bmatrix}\boldsymbol{x}_{ij}^{j} & \boldsymbol{\gamma}_{ij}^{j}\end{bmatrix}^{T}$, the vector superscript j represents the reference frame. If the vector has no superscript, the default reference frame is the inertial frame O.

Reference frames of CDPCR is shown in figure 2. O is the geodetic frame, the frame is fixedly connected with inertial space. The coordinate axis orientation is consistent with the ship frame under the calm sea. S is the ship frame, which is fixedly connected with the ship. The origin S is located in the center of the hull trunk, the x_s-axis coincides with the ship's baseline, the y_s-axis direction from starboard to port, and the z_s-axis direction is determined by the right hand rule. C is the CDPCR framework frame, the coordinate axis orientation are the same as the ship frame. P is the end-motion platform frame, and the origin P is located at the centroid of the motion platform.

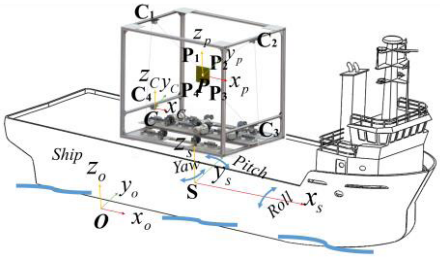

Figure 2. Reference frames of CDPCR.

$\boldsymbol{l}_i$ is the length vector of the *i*-th cable, specifically expressed as

$$\boldsymbol{l}_i=\boldsymbol{c}_i-(\boldsymbol{x}_{\boldsymbol{PO}}+\boldsymbol{p}_i) \tag{1}$$

The above formula is expressed in the frame C:

$$\boldsymbol{l}_i^{C}=\boldsymbol{c}_i^{C}-(\boldsymbol{x}_{PC}^{C}+\boldsymbol{R}_P^{C}\boldsymbol{p}_i^{P}) \tag{2}$$

Further, by derivation of Equation (2).

$$\dot{l}_i\boldsymbol{u}_i^{C}+l_i\dot{\boldsymbol{u}}_i^{C}=\dot{\boldsymbol{c}}_i^{C}-\dot{\boldsymbol{x}}_{PC}^{C}-\left(\dot{\boldsymbol{R}}_P^{C}\boldsymbol{p}_i^{P}+\boldsymbol{R}_P^{C}\dot{\boldsymbol{p}}_i^{P}\right) \tag{3}$$

where $\dot{\boldsymbol{c}}_i^{C}$ and $\dot{\boldsymbol{p}}_i^{P}$ are zero. $\boldsymbol{u}_i^{C}=\boldsymbol{l}_i^{C}/l_i$ is the cable length unit vector.

Multiplying both ends of the Equation (3) by the unit vector $(\boldsymbol{u}_i^C)^T$, according to the rotation matrix derivation formula $\dot{\boldsymbol{R}}_P^C \boldsymbol{p}_i^P = \boldsymbol{\omega}_{PC}^C \times \left(\boldsymbol{R}_P^C \boldsymbol{p}_i^P\right)$, and the velocity vector can be obtained:

$$\dot{l}_i = -(\boldsymbol{u}_i^C)^T \dot{\boldsymbol{x}}_{PC}^C - \left(\left(\boldsymbol{R}_P^C \boldsymbol{p}_i^P\right) \times \boldsymbol{u}_i^C\right)^T \boldsymbol{\omega}_{PC}^C = -\begin{pmatrix} (\boldsymbol{u}_i^C)^T & \left(\left(\boldsymbol{R}_P^C \boldsymbol{p}_i^P\right) \times \boldsymbol{u}_i^C\right)^T \end{pmatrix} \begin{pmatrix} \dot{\boldsymbol{x}}_{PC}^C \\ \boldsymbol{\omega}_{PC}^C \end{pmatrix} \tag{4}$$

Further rearranging Equation (4) can get:

$$\dot{\boldsymbol{l}} = -\tilde{\boldsymbol{J}} \dot{\boldsymbol{x}}_{PC}^C \tag{5}$$

where $\tilde{\boldsymbol{J}}$ is the system Jacobian in local frame.

$$\tilde{\boldsymbol{J}} = \begin{bmatrix} (\boldsymbol{u}_1^C)^T & \left(\left(\boldsymbol{R}_P^C \boldsymbol{p}_1^P\right) \times \boldsymbol{u}_1^C\right)^T \\ (\boldsymbol{u}_2^C)^T & \left(\left(\boldsymbol{R}_P^C \boldsymbol{p}_2^P\right) \times \boldsymbol{u}_2^C\right)^T \\ (\boldsymbol{u}_3^C)^T & \left(\left(\boldsymbol{R}_P^C \boldsymbol{p}_3^P\right) \times \boldsymbol{u}_3^C\right)^T \\ (\boldsymbol{u}_4^C)^T & \left(\left(\boldsymbol{R}_P^C \boldsymbol{p}_4^P\right) \times \boldsymbol{u}_4^C\right)^T \end{bmatrix} \tag{6}$$

3.2. Dynamic Model

The CDPCR dynamic model considering ship excitation was established based on Newton-Euler method. Dynamic coefficients of CDPCR are shown in figure 3.

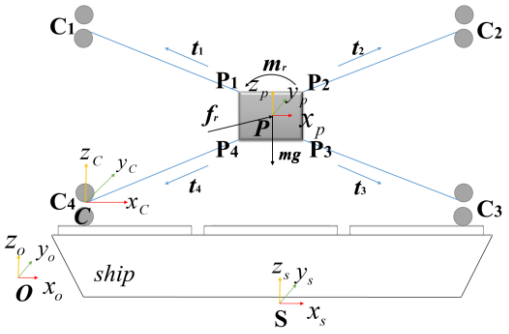

Figure 3. Dynamic coefficients of CDPCR.

According to the above definition, the expression of coordinate P can be expanded as follows

$$\boldsymbol{x}_{PO}^O = \boldsymbol{x}_{SO}^O + \boldsymbol{R}_S^O \boldsymbol{x}_{PS}^S \tag{7}$$

The velocity and coordinate P can be obtained by taking the first and second derivatives of both sides of Equation (7) respectively

$$\dot{\boldsymbol{x}}_{\boldsymbol{PO}}^{\boldsymbol{O}} = \dot{\boldsymbol{x}}_{\boldsymbol{SO}}^{\boldsymbol{O}} + \left[\boldsymbol{\omega}_{\boldsymbol{SO}}^{\boldsymbol{O}}\times\right]\boldsymbol{R}_{\boldsymbol{S}}^{\boldsymbol{O}}\boldsymbol{x}_{\boldsymbol{PS}}^{\boldsymbol{S}} + \boldsymbol{R}_{\boldsymbol{S}}^{\boldsymbol{O}}\dot{\boldsymbol{x}}_{\boldsymbol{PS}}^{\boldsymbol{S}} \tag{8}$$

where $\left[\boldsymbol{\omega}_{\boldsymbol{SO}}^{\boldsymbol{O}}\times\right]$ is the antisymmetric matrix of ω_{SO}^{O}.

$$\ddot{\boldsymbol{x}}_{\boldsymbol{PO}}^{\boldsymbol{O}} = \ddot{\boldsymbol{x}}_{\boldsymbol{SO}}^{\boldsymbol{O}} + \left[\dot{\boldsymbol{\omega}}_{\boldsymbol{SO}}^{\boldsymbol{O}}\times\right]\boldsymbol{R}_{\boldsymbol{S}}^{\boldsymbol{O}}\boldsymbol{x}_{\boldsymbol{PS}}^{\boldsymbol{S}} + \left[\boldsymbol{\omega}_{\boldsymbol{SO}}^{\boldsymbol{O}}\times\right]\left[\boldsymbol{\omega}_{\boldsymbol{SO}}^{\boldsymbol{O}}\times\right]\boldsymbol{R}_{\boldsymbol{S}}^{\boldsymbol{O}}\boldsymbol{x}_{\boldsymbol{PS}}^{\boldsymbol{S}} + 2\left[\boldsymbol{\omega}_{\boldsymbol{SO}}^{\boldsymbol{O}}\times\right]\boldsymbol{R}_{\boldsymbol{S}}^{\boldsymbol{O}}\dot{\boldsymbol{x}}_{\boldsymbol{PS}}^{\boldsymbol{S}} + \boldsymbol{R}_{\boldsymbol{S}}^{\boldsymbol{O}}\ddot{\boldsymbol{x}}_{\boldsymbol{PS}}^{\boldsymbol{S}} \tag{9}$$

Similarly, angular velocity and angular acceleration can be written as

$$\boldsymbol{\omega}_{\boldsymbol{PO}}^{\boldsymbol{O}} = \boldsymbol{R}_{\boldsymbol{S}}^{\boldsymbol{O}}\boldsymbol{\omega}_{\boldsymbol{SO}}^{\boldsymbol{S}} + \boldsymbol{R}_{\boldsymbol{S}}^{\boldsymbol{O}}\boldsymbol{\omega}_{\boldsymbol{PS}}^{\boldsymbol{S}} \tag{10}$$

$$\dot{\boldsymbol{\omega}}_{\boldsymbol{PO}}^{\boldsymbol{O}} = \boldsymbol{R}_{\boldsymbol{S}}^{\boldsymbol{O}}\dot{\boldsymbol{\omega}}_{\boldsymbol{SO}}^{\boldsymbol{S}} + \left[\boldsymbol{\omega}_{\boldsymbol{SO}}^{\boldsymbol{O}}\times\right]\boldsymbol{R}_{\boldsymbol{S}}^{\boldsymbol{O}}\boldsymbol{\omega}_{\boldsymbol{PS}}^{\boldsymbol{S}} + \boldsymbol{R}_{\boldsymbol{S}}^{\boldsymbol{O}}\dot{\boldsymbol{\omega}}_{\boldsymbol{PS}}^{\boldsymbol{S}} \tag{11}$$

The resultant force and torque on the motion platform can be expressed as

$$\begin{cases} m\ddot{\boldsymbol{x}}_{\boldsymbol{PO}}^{\boldsymbol{O}} = \sum_{i=1}^{m}\boldsymbol{u}_i t_i + m\boldsymbol{g} + \boldsymbol{f}_r \\ \boldsymbol{I}\dot{\boldsymbol{\omega}}_{\boldsymbol{PO}}^{\boldsymbol{O}} + \boldsymbol{\omega}_{\boldsymbol{PO}}^{\boldsymbol{O}}\times\left(\boldsymbol{I}\boldsymbol{\omega}_{\boldsymbol{PO}}^{\boldsymbol{O}}\right) = \sum_{i=1}^{m} t_i\left(\boldsymbol{p}_i\times\boldsymbol{u}_i\right) + \boldsymbol{m}_r \end{cases} \tag{12}$$

where $\boldsymbol{I} = \boldsymbol{R}_{\boldsymbol{S}}^{\boldsymbol{O}}\boldsymbol{R}_{\boldsymbol{P}}^{\boldsymbol{C}}\boldsymbol{I}_{\boldsymbol{PP}}\left(\boldsymbol{R}_{\boldsymbol{P}}^{\boldsymbol{C}}\right)^{\boldsymbol{T}}\left(\boldsymbol{R}_{\boldsymbol{S}}^{\boldsymbol{O}}\right)^{\boldsymbol{T}}$ is the inertial matrix in O frame. $\boldsymbol{I}_{\boldsymbol{PP}} = \begin{bmatrix} I_{xx} & -I_{xy} & -I_{xz} \\ -I_{yx} & I_{yy} & -I_{yz} \\ -I_{zx} & -I_{zy} & I_{zz} \end{bmatrix}$ is the inertial matrix in P frame. t_i is the tension vector. $\boldsymbol{f}_r$ and $\boldsymbol{m}_r$ are external disturbance forces and torques.

The dynamic equation of the system in the geodetic frame can be obtained by combining the above two equation

$$\boldsymbol{M}\ddot{\boldsymbol{X}}_{\boldsymbol{PO}} + \boldsymbol{C}\dot{\boldsymbol{X}}_{\boldsymbol{PO}} - \boldsymbol{G} - \boldsymbol{F}_r = \boldsymbol{J}^{\boldsymbol{T}}\boldsymbol{T} \tag{13}$$

where $\boldsymbol{M} = \begin{bmatrix} m\boldsymbol{E}_{3\times3} & \boldsymbol{0}_{3\times3} \\ \boldsymbol{0}_{3\times3} & \boldsymbol{I} \end{bmatrix}$, $\boldsymbol{G} = \begin{bmatrix} 0 & 0 & mg & 0 & 0 & 0 \end{bmatrix}^{\boldsymbol{T}}$ and $\boldsymbol{C} = \begin{bmatrix} \boldsymbol{0}_{3\times3} & \boldsymbol{0}_{3\times3} \\ \boldsymbol{0}_{3\times3} & \left[\boldsymbol{\omega}_{\boldsymbol{PO}}^{\boldsymbol{O}}\times\right]\boldsymbol{I} \end{bmatrix}$.

$\boldsymbol{J} = \begin{bmatrix} \left(\boldsymbol{u}_1^{\boldsymbol{O}}\right)^{\boldsymbol{T}} & \left(\boldsymbol{P}_1^{\boldsymbol{O}}\times\boldsymbol{u}_1^{\boldsymbol{O}}\right)^{\boldsymbol{T}} \\ \left(\boldsymbol{u}_2^{\boldsymbol{O}}\right)^{\boldsymbol{T}} & \left(\boldsymbol{P}_2^{\boldsymbol{O}}\times\boldsymbol{u}_2^{\boldsymbol{O}}\right)^{\boldsymbol{T}} \\ \left(\boldsymbol{u}_3^{\boldsymbol{O}}\right)^{\boldsymbol{T}} & \left(\boldsymbol{P}_3^{\boldsymbol{O}}\times\boldsymbol{u}_3^{\boldsymbol{O}}\right)^{\boldsymbol{T}} \\ \left(\boldsymbol{u}_4^{\boldsymbol{O}}\right)^{\boldsymbol{T}} & \left(\boldsymbol{P}_4^{\boldsymbol{O}}\times\boldsymbol{u}_4^{\boldsymbol{O}}\right)^{\boldsymbol{T}} \end{bmatrix}$ is the Jacobian in global frame.

The relationship between $\boldsymbol{J}$ and $\tilde{\boldsymbol{J}}$ can be expressed as

$$\boldsymbol{J} = \tilde{\boldsymbol{J}}\boldsymbol{S}^{T} \tag{14}$$

where $\boldsymbol{S} = \begin{bmatrix} \boldsymbol{R}_S^O & 0_{3\times3} \\ 0_{3\times3} & \boldsymbol{R}_S^O \end{bmatrix}$.

Further, another form of the dynamic model can be obtained:

$$\tilde{\boldsymbol{J}}^{T}\boldsymbol{T} = \boldsymbol{S}^{-1}\left(\boldsymbol{M}\ddot{\boldsymbol{X}}_{PO} + \boldsymbol{C}\dot{\boldsymbol{X}}_{PO} - \boldsymbol{G} - \boldsymbol{F}_r\right) = \boldsymbol{M}_S\ddot{\boldsymbol{X}}_{PS}^{S} + \boldsymbol{C}_S - \boldsymbol{G} + \boldsymbol{F}_s \tag{15}$$

where $\boldsymbol{M}_S = \begin{bmatrix} m\boldsymbol{E}_{3\times3} & 0_{3\times3} \\ 0_{3\times3} & \boldsymbol{R}_P^S\boldsymbol{I}_{PP}\boldsymbol{I}_{PS} \end{bmatrix}$ is the inertia term. $\boldsymbol{C}_S$ is the hull interference and Coriolis terms,

$$\boldsymbol{C}_S = \begin{bmatrix} m\ddot{\boldsymbol{x}}_{SO}^{S} + m\left(\left[\dot{\boldsymbol{\omega}}_{SO}^{S}\times\right] + \left[\boldsymbol{\omega}_{SO}^{S}\times\right]\left[\boldsymbol{\omega}_{SO}^{S}\times\right]\right)\boldsymbol{x}_{PS}^{S} + 2m\left[\boldsymbol{\omega}_{SO}^{S}\times\right]\dot{\boldsymbol{x}}_{PS}^{S} \\ \boldsymbol{R}_P^S\boldsymbol{I}_{PP}\left(\dot{\boldsymbol{I}}_{PS}\dot{\boldsymbol{\psi}}_{PS} + \boldsymbol{R}_S^P\left[\boldsymbol{\omega}_{SO}^{S}\times\right]\boldsymbol{R}_P^S\boldsymbol{I}_{PS}\dot{\boldsymbol{\psi}}_{PS} + \boldsymbol{R}_S^P\dot{\boldsymbol{\omega}}_{SO}^{S}\right) + \boldsymbol{R}_P^S\left[\left(\boldsymbol{R}_S^P\boldsymbol{\omega}_{SO}^{S} + \boldsymbol{I}_{PS}\dot{\boldsymbol{\psi}}_{PS}\right)\times\right]\boldsymbol{I}_{PP}\left(\boldsymbol{R}_S^P\boldsymbol{\omega}_{SO}^{S} + \boldsymbol{I}_{PS}\dot{\boldsymbol{\psi}}_{PS}\right) \end{bmatrix}$$

$\boldsymbol{F}_s$ is external interference,

$$\boldsymbol{F}_S = \begin{bmatrix} \left(\boldsymbol{E} - \boldsymbol{R}_O^S\right)m\boldsymbol{g} - \boldsymbol{R}_O^S\boldsymbol{f}_r + m\boldsymbol{R}_O^S\ddot{\boldsymbol{x}}_{SO}^{O} - m\ddot{\boldsymbol{x}}_{SO}^{S} \\ -\boldsymbol{R}_O^S\boldsymbol{m}_r \end{bmatrix} \tag{16}$$

3.3. Tension Optimization

The cable tension obtained by directly solving the dynamic model may have negative values, which is inconsistent with actual experience. The cable tension optimization algorithm is used to optimize the solved cable tension

$$\boldsymbol{T} = \boldsymbol{T}_S + \boldsymbol{T}_H \tag{17}$$

$$\boldsymbol{T}_S = \boldsymbol{J}^{+}\left(\boldsymbol{M}\ddot{\boldsymbol{X}}_{PO} + \boldsymbol{C}\dot{\boldsymbol{X}}_{PO} - \boldsymbol{G} - \boldsymbol{F}_r\right) \tag{18}$$

$$\boldsymbol{T}_H = \boldsymbol{N}\left(\boldsymbol{J}\right)\lambda \tag{19}$$

where $\boldsymbol{N}\left(\boldsymbol{J}\right)$ is the null space vector of the matrix $\boldsymbol{J}$. $\boldsymbol{J}^{T+} = \boldsymbol{J}\left(\boldsymbol{J}^{T}\boldsymbol{J}\right)^{-1}$ is the pseudo-inverse matrix of the structural matrix $\boldsymbol{J}$.

The least-variance method was used to optimize, the following tension optimization model was established

$$\begin{cases} \min \quad F(\lambda)=\dfrac{1}{m}\left[\sum_{i=1}^{m}\left(T_i-\boldsymbol{E}(\mathrm{T})\right)^2\right] \\ s.t. \quad \boldsymbol{M}\ddot{\boldsymbol{X}}_{\boldsymbol{PO}}+\boldsymbol{C}\dot{\boldsymbol{X}}_{\boldsymbol{PO}}-\boldsymbol{G}-\boldsymbol{F}_r=\boldsymbol{J}^T\boldsymbol{T} \\ \underline{\lambda}\le\lambda\le\overline{\lambda} \end{cases} \tag{20}$$

where $\underline{\lambda}=\min\limits_{1\le i\le m}\left(\max\limits_{1\le i\le m}\left(\dfrac{T_{i,\min}-T_{S,i}}{N(J)_i},\dfrac{T_{i,\max}-T_{S,i}}{N(J)_i}\right)\right)$ is the lower limit of λ, $\overline{\lambda}=\max\limits_{1\le i\le m}\left(\min\limits_{1\le i\le m}\left(\dfrac{T_{i,\min}-T_{S,i}}{N(J)_i},\dfrac{T_{i,\max}-T_{S,i}}{N(J)_i}\right)\right)$ is the upper limit of the λ. $\boldsymbol{E}(\mathrm{T})=\left(\boldsymbol{T}_{i,\min}+\boldsymbol{T}_{i,\max}\right)/2$ is the mean of tension. $T_{i\min}$ is the minimum pre-tightening force. $T_{i\max}$ is determined by the intensity of the cable.

4. Example Calculation and Analysis

The dynamics model and cable tension optimization model of the CDPCR were established by MATLAB-Simulink, and the virtual prototype model was established by Adams.

4.1. Simulation Parameter Setting

On the premise that the simulation accuracy is not affected, Adams is used to simplify the model of the CDPCR, and Adams-cable module is further used to establish the simulation model. Co-simulation process is shown in figure 4.

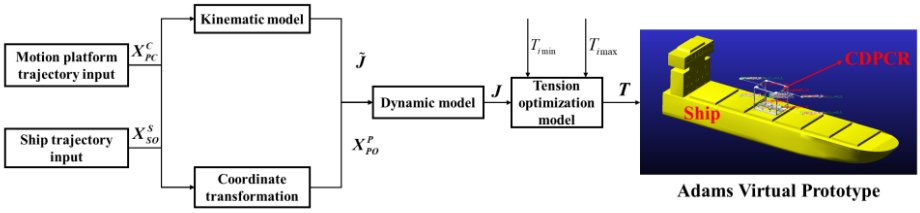

Figure 4. Co-simulation flow chart.

The simulation parameters of the cleaning robot are as follows: parameters related to the motion platform $\boldsymbol{P}_1^{\boldsymbol{P}}=\left[-0.125\quad 0\quad 0.15\right]^{\mathrm{T}}\mathrm{m}$, $\boldsymbol{P}_2^{\boldsymbol{P}}=\left[0.125\quad 0\quad 0.15\right]^{\mathrm{T}}\mathrm{m}$, $\boldsymbol{P}_3^{\boldsymbol{P}}=\left[0.125\quad 0\quad -0.15\right]^{\mathrm{T}}\mathrm{m}$, $\boldsymbol{P}_4^{\boldsymbol{P}}=\left[-0.125\quad 0\quad -0.15\right]^{\mathrm{T}}\mathrm{m}$. Framework parameters $\boldsymbol{C}_1^{\boldsymbol{C}}=\left[0\quad 0\quad 1.4\right]^{\mathrm{T}}\mathrm{m}$, $\boldsymbol{C}_2^{\boldsymbol{C}}=\left[1.9\quad 0\quad 1.4\right]^{\mathrm{T}}\mathrm{m}$, $\boldsymbol{C}_3^{\boldsymbol{C}}=\left[1.9\quad 0\quad 0\right]^{\mathrm{T}}\mathrm{m}$, $\boldsymbol{C}_4^{\boldsymbol{C}}=\left[0\quad 0\quad 0\right]^{\mathrm{T}}\mathrm{m}$. Motion platform mass $m=5\mathrm{kg}$. The moment of inertia

$\boldsymbol{I}_{PP} = \mathrm{diag}[0.03\ 0.03\ 0.06]\mathrm{kg}\cdot\mathrm{m}^2$, Acceleration of gravity g = -9.8kg/m^2. Upper limit of cable tension $T_{i,\max} = 450\mathrm{N}$. Lower limit of cable tension $T_{i,\min} = 10\mathrm{N}$. The simulation time step is set to 1ms.

The initial position and angle of frame S are set to $\boldsymbol{x}_{SO}^{O}(0) = [0\ 0\ 0]^{\mathrm{T}}$ m and $\boldsymbol{\theta}_{SO}^{O}(0) = [0\ 0\ 0]^{\mathrm{T}}$ deg respectively. The initial position and angle of frame P are set to $\boldsymbol{x}_{PO}^{O}(0) = [0.2\ 0\ 2.9]^{\mathrm{T}}$ m and $\boldsymbol{\theta}_{PO}^{O}(0) = [0\ 5\ 0]^{\mathrm{T}}$ deg respectively.

4.2. Simulation and Analysis

The planned motion path of frame P relative to frame C is a circular trajectory, which is as follows:

$$\begin{cases} \boldsymbol{x}_{PC}^{C} = 0.38\cos\left(\dfrac{2\pi}{15}\boldsymbol{t}\right) + 0.6 \\ \boldsymbol{z}_{PC}^{C} = 0.38\sin\left(\dfrac{2\pi}{15}\boldsymbol{t}\right) + 0.7 \\ \boldsymbol{\theta}_{PC}^{C} = 0 \end{cases} \tag{21}$$

The motion simulation under multi-degree-of-freedom excitation is carried out. The motion applied by the waves to the ship is given as:

$$\begin{cases} R_x = 6\sin\left((\pi/3)t\right) \\ R_y = 3\sin\left((\pi/3)t\right) \\ R_z = 0.5\sin\left((\pi/3)t\right) \end{cases} \tag{22}$$

Cable tension optimization comparison is shown in figure 5. As can be seen from figure 5(a), the cable tension change curve is not smooth, and there are negative values. The change in cable tension is not satisfied with actual experience, so the cable tension needs to be optimized. Obtained from figure 5(b), the cable tension curve is continuous and smooth after optimization. At the initial moment, due to the gravity of the motion platform, the tension of cable 1 and 2 is greater than the tension of cable 3 and 4. Consistent with actual experience.

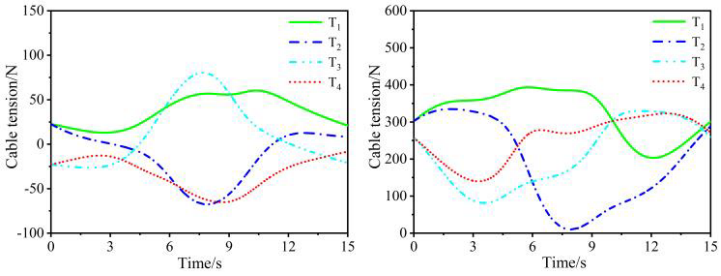

(a) Before tension optimization **(b)** After tension optimization

Figure 5. Cable tension optimization comparison.

The optimized cable tension is used as Adams input. Cable length comparison is shown in figure 6, the Target cable length is given by the kinematic model, and the Actual cable length is the Adams output. In the case of the dynamic verification model as an open-loop system, the optimized cable tension value is input to the virtual prototype, and the actual cable length change is basically the same as the Target length. The maximum error was 0.15m at cable 2, in the case of open-loop, the precision can meet the requirements.

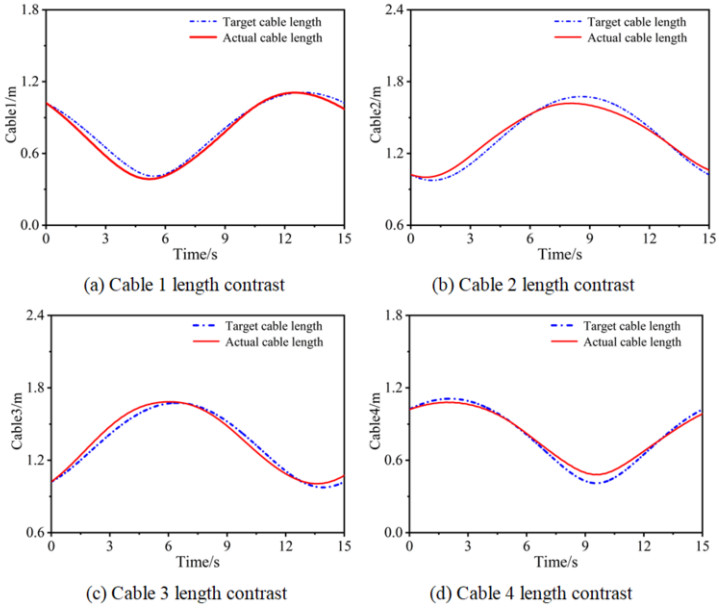

Figure 6. Cable length comparison.

Track tracking effect is shown in figure 7. As can be seen from figures 7(a) and 7(b), the displacement tracking effect is good. The ship shakes under the action of wave excitation, resulting in a large angle tracking error. Because the roll Angle is too large, the tracking effect in X direction is worse than that in Y direction. The maximum error of X direction tracking is 0.025m, the maximum error of Z direction tracking is 0.013m,

and the maximum error of Angle tracking is 0.48°. The mean value of the overall error is small, which verifies that the established model is accurate and reasonable.

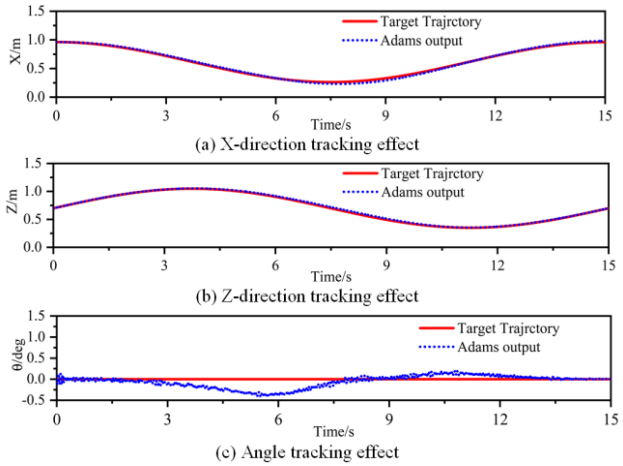

Figure 7. Track tracking effect.

5. Conclusion

This paper proposed a new type of marine cleaning robot. Considering the effect of the ship's base motion and external disturbances, the dynamic model of the CDPCR system is established based on the Newton-Euler method. Furthermore, the cable tension is optimized by the method of minimum variance based on the correlation force, the optimized tension changes continuously and uniformly within the extreme value. Finally, the validity of the proposed theory is verified by virtual prototype simulation. The results show that the trajectory comparison effect is good under the wave excitation, which indicates that the proposed theory is accurate and effective. Relevant research results can provide theoretical basis for CDPR control strategy research and ship application.

Acknowledgments

The author(s) would like to acknowledge the support provided by the National Natural Science Foundation of China (Project No. 52101396), the China Fundamental Research Funds for the Central Universities (Project No. 3132022207, 3132022341), and the National Key Research and Development Program of China (Project No. 2018YFC0309003).

References

[1] Guerra-Contreras A, Camacho-Ramírez A, Olvera-Sosa M, et al. Evaluation of a rapid and long-effective pickling method for iron rust removal on metallic surfaces using carboxylic acid-based polymers. Journal of Polymer Research. 2021; 28(4): 1-13.

[2] Sun L, Gong, Y. J, Zhang Z. M, et al. Hardware technology research on ultra-high pressure water jet ship rust control system based on PLC. Applied Mechanics and Materials. 2013; 365: 812-816.
[3] Jin XJ, Jung J, Ko SY, et al. Geometric parameter calibration for a cable-driven parallel robot based on a single one-dimensional laser distance sensor measurement and experimental modeling. Sensors. 2018; 18(7): 2392.
[4] Khosravi MA, Taghirad HD. Dynamic analysis and control of cable driven robots with elastic cables. Transactions of the Canadian Society for Mechanical Engineering. 2011; 35(4): 543-557.
[5] Runciman M, Avery J, Zhao M, et al. Deployable, variable stiffness, cable driven robot for minimally invasive surgery. Frontiers in Robotics and AI. 2020: 141.
[6] Zi B, Wang N, Qian S, et al. Design, stiffness analysis and experimental study of a cable-driven parallel 3D printer. Mechanism and Machine Theory. 2019; 132: 207-222.
[7] Jiang Q and Kumar V. The inverse kinematics of cooperative transport with multiple aerial robots. IEEE Transactions on Robotics. 2013; 29(1): 136-145.
[8] Horoub MM, Hassan M, Hawwa MA. Workspace analysis of a Gough-Stewart type cable marine platform subjected to harmonic water waves. Mechanism and Machine Theory. 2018; 120: 314-325.
[9] Rushton M, Jamshidifar H, Khajepour A. Multiaxis reaction system (MARS) for vibration control of planar cable-driven parallel robots. IEEE Transactions on Robotics. 2019; 35(4): 1039-1046.
[10] Du J, Agrawal SK. Dynamic modeling of cable-driven parallel manipulators with distributed mass flexible cables. Journal of Vibration and Acoustics. 2015; 137(2).
[11] Zhao Z, Zhang L, Nan H, et al. System modeling and motion control of a cable-driven parallel platform for underwater camera stabilization. IEEE Access. 2021; 9: 132954-132966.
[12] Pott A. An improved force distribution algorithm for over-constrained cable-driven parallel robots. Computational Kinematics. Springer: Dordrecht. 2014; p.139-146.
[13] Borgstrom PH, Borgstrom NP, Stealey MJ, et al. Design and implementation of NIMS3D, a 3-D cabled robot for actuated sensing applications. IEEE Transactions on Robotics. 2009; 25(2): 325-339.